Research on End Effect of Linear Induction Machine for High-Speed Industrial Transportation

Junyong Lu and Weiming Ma, *Member, IEEE*

***Abstract*—Due to the difference of movement and boundary conditions between long-primary double-sided linear induction motors (DSLIMs) and short-primary DSLIMs, the longitudinal end effect is different. This paper analyzes the dynamic longitudinal end effect of long-primary LIMs according to the basic principle and electromagnetic field theory and explains the difference of magnetic field traveling wave and its influence between these two kinds of DSLIM. The equivalent circuit model and correction factors considering the end effect are described through theory analysis. To verify the validity of the model, 3-D field analysis by Ansoft 3-D is implemented, and the field distribution is presented. The analysis results have a good agreement with the results where the end effect is considered than that where the end effect is not considered. A useful conclusion is that, with proper selection of the secondary poles and proper attention to the slip that the machine is operating at, the end effect will have a much smaller influence than that in the short-primary DSLIM. It provides a good way for this kind of machine design and industrial application in the future.**

***Index Terms*—Double-sided linear induction motor (DSLIM), end effect, equivalent circuit model, high speed, long primary.**

I. Introduction

COMPARED with linear permanent-magnet brushless dc machines or linear synchronous machines for high-speed industrial transportation, the linear induction machine (LIM) is more realizable because of its simple structure and low cost. Recently, typical applications of the LIM in passenger transport have been the No. 4 and No. 5 linear metro in Guangzhou, China. However, there are two types of LIM according to the length of the primary and the secondary, namely the long-primary member LIM and the short-primary member one, as shown in Fig. 1. Most research studies about the end effect have been experienced in a short-primary double-sided LIM (DSLIM), but a long-primary DSLIM will have different end effects because the movement and the computational band are different compared with the short-primary DSLIM. In the short-primary DSLIM, the magnetic field traveling is running forward with the same speed as the primary. Under these high-speed conditions, the magnetic field on the entry end of the primary is seriously degraded, and this degradation would grow with increasing speed. However, in the long-primary DSLIM, a stationary primary produces a magnetic field that sweeps forward over the secondary with slip speed. This paper analyzes the dynamic end effect of the long-primary DSLIM according to the basic principle and electromagnetic field theory and presents the equivalent circuit and longitudinal end effect factor. Some important conclusions are derived, and many useful characteristics are obtained for this type of DSLIM.

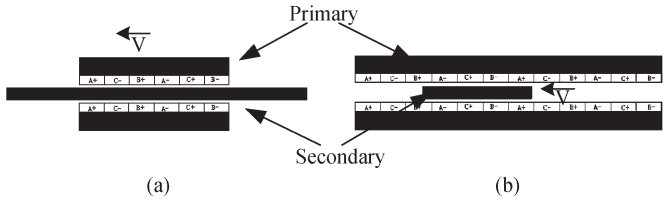

Fig. 1. Two-dimensional model of two types of DSLIM. (a) Short-primary DSLIM. (b) Long-primary DSLIM.

II. Basic Structure and Analytical Model

Fig. 2 shows the basic structure of the long-primary DSLIM for high-speed transportation. The primary is located along the track, and the secondary is vertically mounted on the undercarriage, which would decrease the whole weight of the train. The fundamental advantage of DSLIMs is the elimination of the normal attractive force between the primary and the secondary because the secondary is nonferromagnetic.

For a high-speed linear motor, the pole pitch is generally very large, so it can use a 1-D model to analyze the characteristic of DSLIMs.

To simplify the model, some assumptions are made.

1) The field distribution is quasi-stationary.
2) The permeability of stator core is infinite, so the reluctance of the stator core could be neglected.
3) The current is only along the z direction.
4) Time harmonic effects are neglected.
5) The field outside the end yoke is equal to zero.

According to Ampere's law, the current equation is

$$g_e \frac{\partial H_y}{\partial x} = J_{s1} + J_{r1} \tag{1}$$

where g_e is the equivalent length of the air gap and J_{s1} and J_{r1} are the surface current density of the primary and the secondary, respectively.

Manuscript received December 18, 2009; revised August 17, 2010; accepted October 2, 2010. Date of publication October 28, 2010; date of current version January 7, 2011. This work was supported by Science Foundation of Innovation Research Group of National Natural Science Foundation of China (50721063).

The authors are with the Research Institute of Power Electronic Technology, Naval University of Engineering, Wuhan 430033, China (e-mail: jylu@xinhuanet.com; maweimin@public.wh.hb.cn).

Color versions of one or more of the figures in this paper are available online at http://ieeexplore.ieee.org.

Digital Object Identifier 10.1109/TPS.2010.2085089

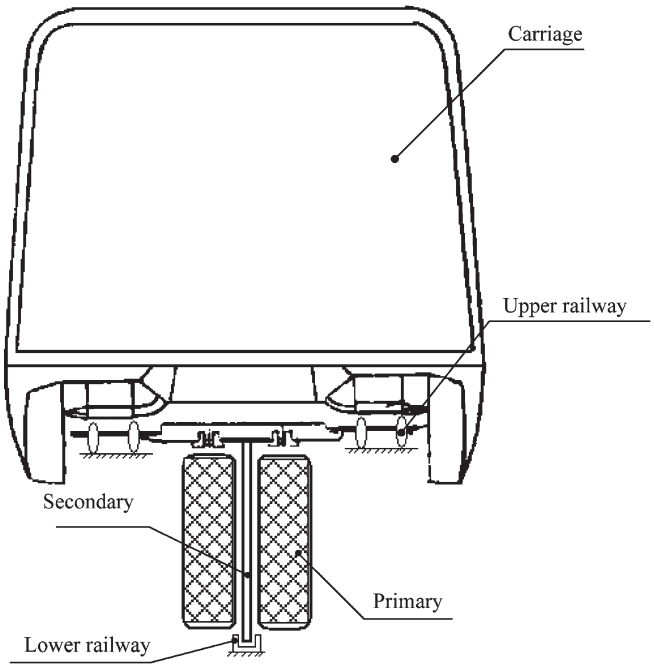

Fig. 2. DSLIM with short secondary mounted on the undercarriage.

J_{s1} can be expressed as follows:

$$J_{s1} = J_{sm} e^{j(\omega t - \beta x)} \tag{2}$$

where ω is the angular frequency, J_{sm} is the magnitude of the surface current density, τ is the pole pitch, and the value of β is π/τ.

J_{r1} can be expressed as follows:

$$J_{r1} = \sigma_s (E_z + V_x B_y) \tag{3}$$

where σ_s, E_z, and V_x are the surface conductivity, back EMF, and velocity of the secondary, respectively. B_y is the magnetic flux density of the air gap.

According to (1)–(3) and applying Faraday's law, the magnetic field intensity of the air gap (H_y) can be expressed as follows:

$$\frac{\partial^2 H_y}{\partial x^2} - \mu_0 \frac{\sigma_s}{g_e} V_x \frac{\partial H_y}{\partial x} - \mu_0 \frac{\sigma_s}{g_e} \frac{\partial H_y}{\partial t} = -j\beta \frac{J_{sm}}{g_e} e^{j(\omega t - \beta x)}. \tag{4}$$

The general solution for (4) is

$$H_y(x,t) = C_1 e^{-\frac{x}{\lambda_1}} e^{j\left(\omega t - \frac{\pi}{\tau_e} x\right)} + C_2 e^{\frac{x}{\lambda_2}} e^{j\left(\omega t + \frac{\pi}{\tau_e} x\right)} + H_{ym} e^{j\left(\omega t - \frac{\pi}{\tau} x + \varphi\right)}. \tag{5}$$

The first two terms are the end effect wave, and the third term is the common magnetic field wave. C_1 and C_2 are the coefficients to be determined, H_{ym} is the magnitude of H_y, τ_e is the pole pitch of the end wave, λ_1 and λ_2 are the penetration depth of the entry terminal and exit terminal end wave, respectively, and μ_0 is the air permeability.

To solve C_1 and C_2, the long-primary DSLIM could be divided into three zones, which are Zone I $(0 < x < 2p\tau)$, Zone II $(-\infty < x < 0)$, and Zone III $(2p\tau < x < +\infty)$. Fig. 3 shows the different partitions and the boundary conditions.

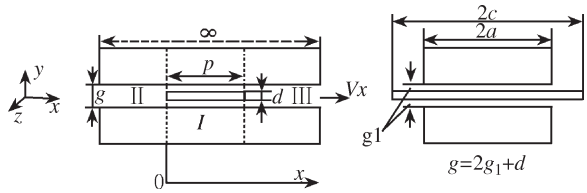

Fig. 3. Computational area of long-primary DSLIM.

P, d, and $2c$ are the pole pair, thickness, and height of the secondary, respectively. $2a$ is the height of the primary.

Zone I is the effective working area of the DSLIM, and the flux field density can be expressed as follows:

$$B_{y_1}(x,t) = C_1 \mu_0 e^{-\frac{x}{\lambda_1}} e^{j\left(\omega t - \frac{\pi}{\tau_e} x\right)} + C_2 \mu_0 e^{\frac{x}{\lambda_2}} e^{j\left(\omega t + \frac{\pi}{\tau_e} x\right)} + \mu_0 H_{ym} e^{j\left(\omega t - \frac{\pi}{\tau} x + \varphi\right)}, \qquad 0 < x < 2p\tau \tag{6}$$

$$H_{ym} = \frac{J_{sm} e^{-j\varphi}}{g_e \beta (sG - j)} \tag{7}$$

where $G = \mu_0 \sigma_s \omega / g_e \beta^2$ in which G is the goodness factor, s is the slip, and $\varphi = \tan^{-1}(1/sG)$.

In the areas of Zone II $(-\infty < x < 0)$ and Zone III $(2p\tau < x < +\infty)$, there is no primary current for the short DSLIM. For the long-primary DSLIM, there is no secondary current in these areas, so $J_{r2} = 0$.

Using (1), the value of H_y in Zone II and Zone III can be derived as follows:

$$H_{y2} = j \frac{J_{sm}}{g_e \beta} e^{j(\omega t - \beta x)}, \qquad (x < 0) \tag{8}$$

$$H_{y3} = j \frac{J_{sm}}{g_e \beta} e^{j[\omega t - \beta(x - 2p\tau)]}, \qquad (x > 2p\tau). \tag{9}$$

The magnetic bands between Zone I and Zone II and Zone II and Zone III are

$$H_{y1}|_{x=0} = H_{y2}|_{x=0} \; H_{y2}|_{x=2p\tau} = H_{y3}|_{x=2p\tau}. \tag{10}$$

Using (5) and (8)–(10), the coefficients to be determined could be resolved

$$\begin{cases} C_1 = \frac{j J_{sm}}{g_e \beta \Delta} \left[\frac{jsG(1 - e^{Q_2})}{1 + jsG} \right] \\ C_2 = \frac{j J_{sm}}{g_e \beta \Delta} \left[\frac{jsG(e^{-Q_1} - 1)}{1 + jsG} \right] \end{cases} \tag{11}$$

where $\Delta = e^{-Q_1} - e^{Q_2}$ and Q_1 and Q_2 can be expressed as follows:

$$\begin{cases} Q_1 = \left(\frac{1}{\lambda_1} + j \frac{\pi}{\tau_e} \right) 2p\tau \\ Q_2 = \left(\frac{1}{\lambda_2} + j \frac{\pi}{\tau_e} \right) 2p\tau. \end{cases} \tag{12}$$

Generally, for high-speed LIMs, there are $\lambda_1 \gg \lambda_2$ and $C_1 \gg C_2$

$$\begin{cases} C_1 \cong \frac{-J_{sm} sG}{g_e \beta (1 + sG)} \\ C_2 \cong 0. \end{cases} \tag{13}$$

Using (5) and (13), the magnetic field distribution of the air gap considering the end effect can be derived.

III. Performance of DSLIM Considering Longitudinal End Effect

According to the aforementioned analysis, the correction factors of the T-type equivalent circuit model can be derived. Defining $C_r(s)$ and $K_r(s)$ as the correction factors of the secondary resistance, $C_x(s)$ and $K_x(s)$ are the correction factors of the magnetizing reactance. $C_r(s)$ and $C_x(s)$ are the correction factors considering the transverse edge effect, which can use the same expressions of the short-primary DSLIM [1]. $K_r(s)$ and $K_x(s)$ are the correction factors considering the longitudinal end effect, which can be expressed as follows:

$$K_r(s) = \frac{sG}{2p\tau\sqrt{1+(sG)^2}} \cdot \frac{K_1^2+K_2^2}{K_1} \tag{14}$$

$$K_x(s) = \frac{1}{2p\tau\sqrt{1+(sG)^2}} \cdot \frac{K_1^2+K_2^2}{K_2} \tag{15}$$

$$\begin{aligned} K_1 =& 2p\tau\cos\delta_b \\ &- N\left[-\frac{1}{\lambda_1}e^{-\frac{2p\tau}{\lambda_1}}\cos(\delta_b-\theta+K_s2p\tau)\right. \\ &+ K_s e^{-\frac{2p\tau}{\lambda_1}}\sin(\delta_b-\theta+K_s2p\tau) \\ &\left.+\frac{1}{\lambda_1}\cos(\delta_b-\theta)-K_s\sin(\delta_b-\theta)\right] \end{aligned} \tag{16}$$

$$\begin{aligned} K_2 =& 2p\tau\sin\delta_b \\ &- N\left[-\frac{1}{\lambda_1}e^{-\frac{2p\tau}{\lambda_1}}\sin(\delta_b-\theta+K_s2p\tau))\right. \\ &- K_s e^{-\frac{2p\tau}{\lambda_1}}\cos(\delta_b-\theta+K_s2p\tau) \\ &\left.+\frac{1}{\lambda_1}\sin(\delta_b-\theta)+K_s\cos(\delta_b-\theta)\right] \end{aligned} \tag{17}$$

where

$$K_s = \frac{\pi}{\tau}-\frac{\pi}{\tau_e} \qquad N = \frac{sG\lambda_1\tau_e\pi}{\tau M\sqrt{\tau_e^2+(\lambda_1\pi)^2}}$$

$$M = \left(\frac{1}{\lambda_1}\right)^2 + K_s^2 \qquad \theta = \tan^{-1}\left(\frac{\lambda_1\pi}{\tau_e}\right)$$

$$\delta_b = \tan^{-1}\left(\frac{1}{sG}\right).$$

It can be derived from (16) and (17) that, the higher the velocity of the long-primary DSLIM, the smaller the influence of the end effect, which is a different characteristic compared with the short-primary DSLIM [2]. Fig. 4 shows the equivalent circuit model of a high-speed DSLIM with end effects. Fig. 5 and Table I show the photograph and parameters of a subscale long-primary DSLIM, respectively.

Fig. 6 gives the curves of the thrust versus the slip at different supply frequencies based on the equivalent circuit model. It can be seen that the impact to the thrust due to the end effect turns smaller with increasing frequency. To the same curve of the thrust versus the slip, when s approaches zero, the results with the end effect have a better agreement than the results without the end effect, which illuminates that the influence of end effect could be neglected when the long-primary DSLIM runs at high-speed mode.

In addition, the influence of end effect has a relationship with the poles of the secondary [3], [7]. Fig. 7(a) and (b) plots the normalized force versus slip for different lengths of the secondary with the end effect and the same secondary without the end effect, respectively. It can be seen that, as the numbers of pole pitch that the secondary spans increase, the influence of end effect weakens.

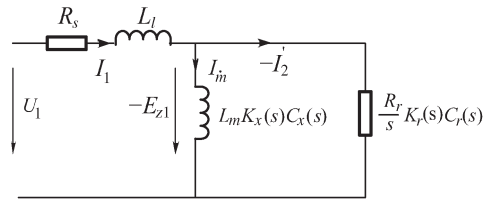

Fig. 4. Equivalent circuit model considering the end effect.

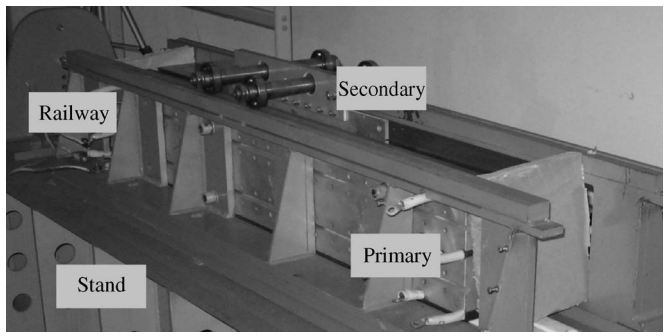

Fig. 5. Prototype machine of a subscale long-primary DSLIM.

TABLE I
Circuit Parameters of LIM

Item	Symbol	Value[Unit]
Resistance of primary	R_s	0.1995 [Ω]
Leakage inductance of stator	L_l	0.5461[mH]
Mutual inductance	M	0.6961 [mH]
Resistance of secondary	R_r	0.07531[Ω]

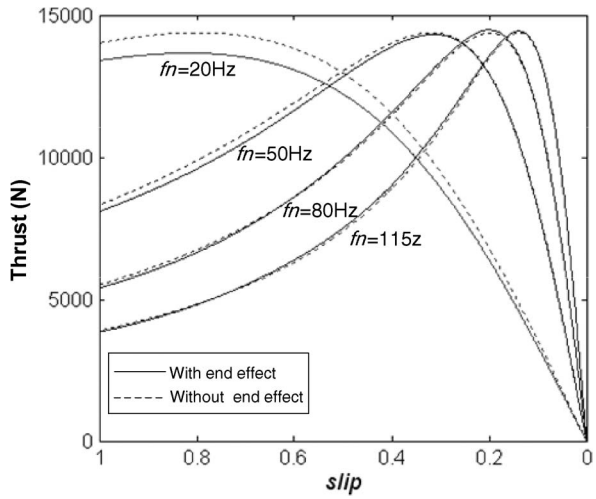

Fig. 6. Thrust versus slip of long-primary DSLIM.

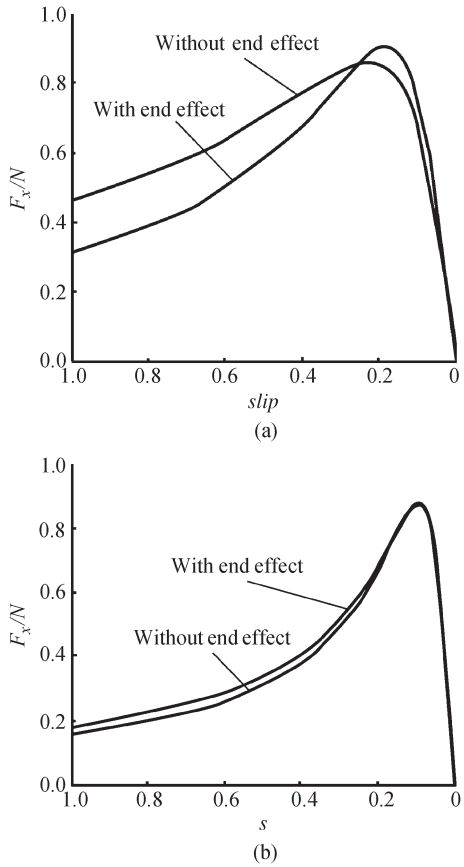

Fig. 7. F_x versus slip at different secondary lengths. (a) secondary length = 2 pole pitches. (b) secondary length = 10 pole pitches.

IV. Three-Dimensional FEA and Test

In order to verify the equivalent circuit model, a 3-D finite-element analysis (FEA) is performed by Ansoft 3-D, as shown in Fig. 8(a). The input is the amplitudes of the phase current, phase angle, and slip frequency. It can be assumed that, if we fix the reference system on the secondary, then the fundamental magnetic field generated by the stator would move as the slip frequency, which means that inputting the slip frequency current into the primary windings can simulate the situation of the secondary running at a high speed. Fig. 8(b) presents the radial field distribution $B_y = f(x)$, when the slip frequency is 20 Hz and the phase current is 430 A. It can be seen that the distortion of the magnetic field is not obvious in the entry and exit ends, which verifies the effectiveness of the aforementioned analysis.

To calculate the curve of the thrust versus slip, 30 runs have been performed, and the frequency of the primary current is different for every run while the current amplitude is kept at 430 A. In order to analyze the performance with the end effect, the curves of the thrust versus slip are also calculated by the lumped model with and without the end effect, as shown in Fig. 9. It can be seen that the difference among the results is very small at a low slip, while it turns larger with the increase of the slip, which implies that the end effect has a larger influence at a low speed while it could be neglected at a high speed. Furthermore, the results with the end effect are closer to the results of the 3-D

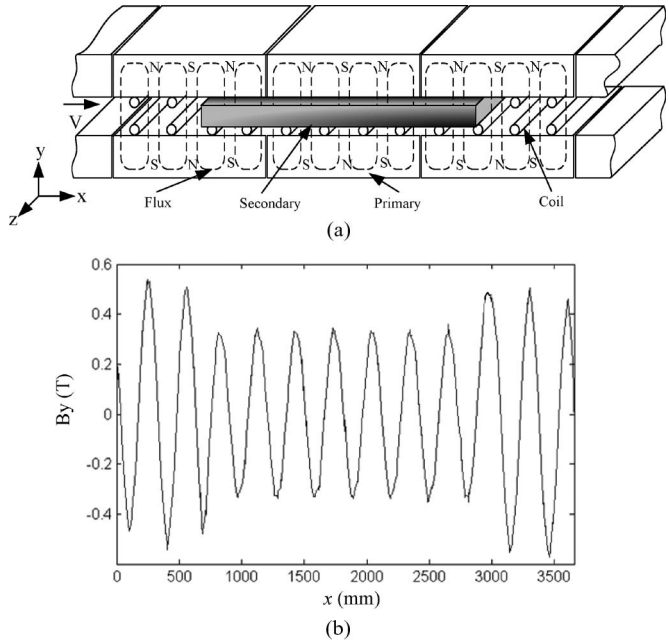

Fig. 8. Model and computational results by Ansoft 3-D. (a) Three-dimensional FEA model of the long-primary DSLIM. (b) Air-gap magnetic field density by Ansoft 3-D.

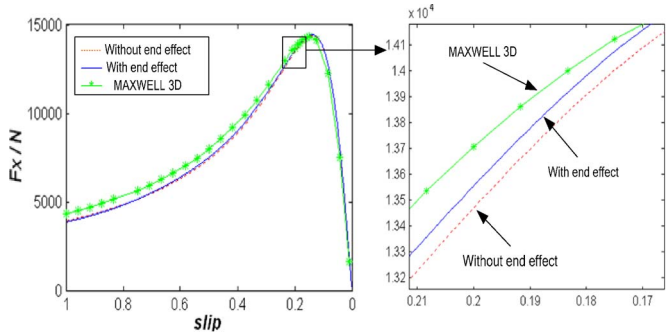

Fig. 9. Thrust versus slip frequency by Ansoft 3-D and equivalent circuit model.

FEA, which verifies the effectiveness of the equivalent circuit model with the end effect.

The experimental thrust versus slip frequency was obtained by the subscale prototype with a locked secondary. The input frequencies into the primary vary from 0 to 120 Hz while the current is kept constant (430 A). To have a visual comparison, all results have been depicted in the same graph, as shown in Fig. 10. It can be seen that the experimental measurements, theoretical analysis, and the FEA results have a good agreement.

V. Conclusion

This paper has analyzed the longitudinal end effect of a high-speed long-primary DSLIM based on the principle and electromagnetic field theory, and the correction factors for the end effect have been obtained. It can be concluded that the influence of the end effect could be neglected when the long-primary DSLIM runs at high-speed mode. Moreover, the influence of end effect turns smaller with the increase of the poles of the secondary. With proper selection of the poles of the secondary

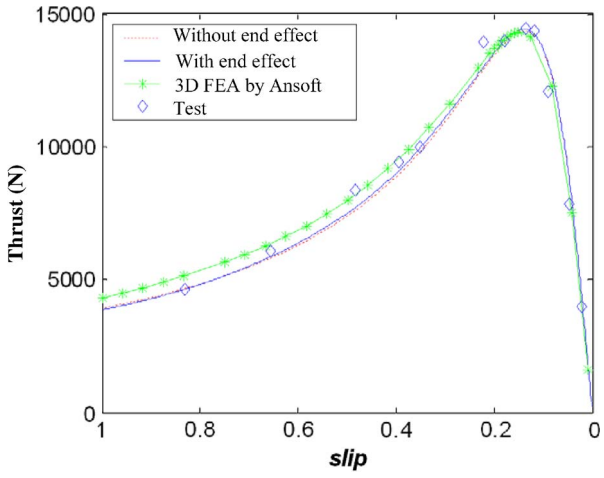

Fig. 10. Test data and computational electromagnetic force.

and proper attention to the slip that the machine is operating at, the end effect will have a much smaller effect than in the short-primary DSLIM. The experimental measurements, theoretical analysis, and the FEA results have a good agreement, which provides a new way for the design and implementation of this kind of machine in high-speed transportation.

REFERENCES

[1] D.-K. Kim and B.-I. Kwon, "A novel equivalent circuit model of linear induction motor based on finite element analysis and its coupling with external circuits," *IEEE Trans. Magn.*, vol. 42, no. 5, pp. 3407–3409, Oct. 2006.

[2] J. Duncan and C. Eng, "Linear induction motor-equivalent-circuit model," *Proc. Inst. Elect. Eng.*, vol. 130, no. 1, pp. 51–57, Jan. 1983.

[3] J. F. Gieras, *Linear Induction Drives*. New York: Oxford Univ. Press, 1994, ch. 2.

[4] L. Xialing, *The Theory and Design Methods Linear Induction Motor Electromagnetic*. Beijing, China: Science Press, 2006, pp. 120–144.

[5] S. Yamamura, *Theory of Linear Induction Motors*. Tokyo, Japan: Univ. Tokyo Press, 1978, ch. 3.

[6] R. M. Pai, I. Boldea, and S. A. Nasar, "A complete equivalent circuit of a linear induction motor with sheet secondary," *IEEE Trans. Magn.*, vol. 21, no. 1, pp. 639–654, Jan. 1988.

[7] A. P. Johnson, "High speed linear induction motor efficiency optimization," M.S. thesis, MIT, Cambridge, MA, 2005.

Junyong Lu was born in Ezhou, China. He received the B.S. degree in electrical engineering from the Naval University of Engineering, Wuhan, China, in 2001, and the M.S. degree from Xi'an Jiaotong University, Xi'an, China, in 2004.

Since 2004, he has been a Docent with the Research Institute of Power Electronic Technology, Naval University of Engineering. His research interests include electrical devices, electric machine design, and its control.

Weiming Ma (M'04) received the B.S. and M.S. degrees in electrical engineering from the Naval University of Engineering, Wuhan, China, in 1982 and 1987, respectively, and the Ph.D. degree from Tsinghua University, Beijing, China, in 1996.

In 2001, he was an Academician with the Chinese Academy of Engineering, Beijing, in 2001. He is currently the Director of the Research Institute of Power Electronic Technique Application with the Naval University of Engineering, where he is also a Professor and Supervisor of doctoral candidates. His research interests include isolated electrical power system, electromagnetic compatibility, and power electronics.